
**Separation Science and Technology**
Publication details, including instructions for authors and subscription information:
http://www.informaworld.com/smpp/title~content=t713708471

# Physicochemical Aspects on Fluoride Adsorption for Removal from Water by Synthetic Hydrous Iron(III) - Chromium(III) Mixed Oxide

Krishna Biswas[a]; Sushanta Debnath[a]; Uday Chand Ghosh[a]
[a] Department of Chemistry, Presidency College, Kolkata, India

Online publication date: 22 February 2010

**To cite this Article** Biswas, Krishna , Debnath, Sushanta and Ghosh, Uday Chand(2010) 'Physicochemical Aspects on Fluoride Adsorption for Removal from Water by Synthetic Hydrous Iron(III) - Chromium(III) Mixed Oxide', Separation Science and Technology, 45: 4, 472 — 485
**To link to this Article: DOI:** 10.1080/01496390903526667
**URL:** http://dx.doi.org/10.1080/01496390903526667

*Separation Science and Technology*, 45: 472–485, 2010

ISSN: 0149-6395 print/1520-5754 online
DOI: 10.1080/01496390903526667

Taylor & Francis
Taylor & Francis Group

# Physicochemical Aspects on Fluoride Adsorption for Removal from Water by Synthetic Hydrous Iron(III) – Chromium(III) Mixed Oxide

**Krishna Biswas, Sushanta Debnath, and Uday Chand Ghosh**
*Department of Chemistry, Presidency College, Kolkata, India*

**Fluoride removal with varying different parameters at $303 \pm 1.6\,K$ and pH $6.5 \pm 0.2$ was investigated by hydrous iron(III)-chromium(III) bimetal oxide. The kinetic and equilibrium data fitted with the pseudo-second order and Langmuir isotherm equations very well ($R^2 = 0.99-1.00$), respectively. The Langmuir capacity ($\theta$) and free energy ($E_{DR}$) of adsorption evaluated were 16.34 ($\pm$0.50) $mg \cdot g^{-1}$ and 15.81 $kJ \cdot mol^{-1}$, respectively. The estimated thermodynamic parameters viz. $\Delta H^0$, $\Delta G^0$, and $\Delta S^0$ indicated that the reaction was endothermic but spontaneous for entropy increase. The small-scale column filtration of high fluoride ($C_0 = 7.37\,mg \cdot L^{-1}$) water gave encouraging results.**

**Keywords** adsorption; column; desorption; fluoride; iron-chromium mixed oxide; kinetics; thermodynamics



## INTRODUCTION

Fluoride is an essential mineral for our dental and bone health at low dose. It is taken through foods and drinks, but excessive intake leads to dental and skeletal fluorosis (1). The major source of fluoride intake is the drinking water. Rural populations of third world countries like India have been using groundwater as the main source of drinking water since long back. The maximum allowed concentration (MAC) for fluoride in drinking water had set to 1.0 and $1.5\,mg \cdot L^{-1}$, respectively, for the tropical and the cooler climatic countries by the World Health Organization (1). Many countries globally have regions where underground aquifers crossed the specified MAC level of fluoride. The source of fluoride in groundwater is due to the release from the minerals like fluorite ($CaF_2$) and fluoroapatite [$3Ca_3(PO_4)_2 \cdot CaF_2$], hosted in the vein of all rocks in sub-surface soil, and mobilizes due to the percolation of water from the upper surface in the underground aquifers. The fluoride release depends on the pH and residence time of percolated water through the soil bed. The bicarbonate rich percolating water is responsible for the acceleration of fluoride release from the minerals for water-mineral interactions under favorable geophysical conditions (2).

The remedial measure of fluoride toxicity is the supply of treated water. However, the shifting of technology requires huge funds for the supply of treated water at remote corners and it is a distant possibility. Thus, the cost-viable and technologically feasible method is an emergent need for third world countries like India.

The popular methods for fluoride removal from contaminated water are coagulation-precipitation, membrane filtration, electro deposition, surface adsorption, and ion exchange. Among them, surface adsorption seems to be the most attractive and selective technique for the reduction of fluoride level from the water because of the requirement of less space, easy operation, affordable cost, and water quality. Numerous natural, synthetic and biomass materials have been investigated as adsorbent (3–39) for the lowering of the fluoride level from the aqueous solution in last few years.

Goethite, a variety of iron(III) oxide and abundant in the earth crust, is one of the naturally occurring water purifier. It had been assumed that the synthetic hydrous iron(III) oxide may be a good fluoride scavenger from the contaminated water. However, the fluoride scavenging ability of synthetic hydrous iron(III) oxide had been found low (32). Thus, we have made the attempt to enhance the fluoride scavenging efficiency of the synthetic iron(III) oxide by incorporating some other metal ion. Thus, zirconium(IV), aluminium(III), and tin(IV) incorporated bimetal iron(III) oxide had been investigated for the fluoride adsorption (34–36). Herein, we have made the attempt to estimate the fluoride adsorption efficiency of chromium(III) incorporated iron(III) oxide from water.

Thus, this manuscript reports herein the results of fluoride adsorption behavior for the removal from water by synthetic hydrous iron(III)-chromium(III) bimetal mixed oxide (HICMO).

Received 6 June 2009; accepted 22 November 2009.
Address correspondence to Uday Chand Ghosh, Department of Chemistry, Presidency College, 86/1 College Street, Kolkata-700073, India. Tel.: 91-33-2241-3893; Fax: 91-33-2241-3893. E-mail: ucghosh@yahoo.co.in

## MATERIALS AND METHODS

### Synthesis of HICMO

The material, HICMO, was synthesized by the co-precipitation method. Here, aqueous ammonia (1:1) was added slowly to the hot (~80°C) well-mixed (agitation speed: ~300 rpm) solution of 0.1 M $FeCl_3$(in 0.1 M HCl) and 0.1 M $CrCl_3$(in 0.1 M HCl) (v/v = 1:1). Addition of ammonia (1:1) was continued until the pH of the solution including the precipitate became 6.2 (±0.2). Aging precipitate with the mother liquid for 3 days, it was filtered, washed with deionised water, and dried in an air-oven (65 to 75°C).

The dried solid lumps when treated with cold water separated to the small particles. After air-drying, particles of dimension ranged in 0.140–0.290 mm were screened out, and homogenized at some pre-fixed pH to be used for conducting experiments.

### Reagents

Sodium fluoride (AR, BDH) was used to prepare a stock solution (1000 mg $F^- \cdot dm^{-3}$). Sodium 2-(para sulfo phenylazo)-1,8-dihydroxy-3,6-naphthalene disulfonate (SPADNS) (G. R.) and zirconium oxychloride octahydrate (L. R.) used for the colorimetric analysis of fluoride were procured from E. Merck India Ltd. (Mumbai), India.

### Instruments

The instruments used for collecting the data were

(i) UV-Vis spectrophotometer (Hitachi model U-3210) for colorimetric analysis of fluoride (40),
(ii) pH meter (model LI-127) made of ELICO (India) for pH analysis,
(iii) Jasco 680 plus spectrophotometer for the Föurier transform infrared (FTIR) spectra,
(iv) Phillips X-ray diffractometer for the powder X-ray diffraction (XRD) analysis,
(v) Setaram Analyzer in argon gas atmosphere at a heating rate 20°C $min^{-1}$ over a temperature range up to 900°C for thermogravimatric (TG) and differential thermal (DT) analyses,
(vi) scanning electron microscope (Vega Tescan, Oxford Instruments) for the scanning electron microscopic (SEM) image, and
(vii) transmission electron microscope (FEI, model Tecnai S Twin) for the TEM image of HICMO.

### Zero Point pH

The zero point surface charge pH ($pH_{zpc}$) value of the synthetic mixed oxide was analyzed using the pH drift method as described by Babic et al. (41).

### Adsorption Experiments

Fluoride adsorption experiments were carried out in polypropylene bottles of capacity 250 ml into which 50 ml aqueous solution of the solute, adjusted ionic strength (I) at 0.01 M with 1.0 M $NaNO_3$ was taken with 0.1 g of HICMO. Initial pH ($pH_i$) of the working solution was adjusted with $HNO_3$ and/or NaOH to the designated value. Then, the reaction mixtures were agitated (speed: 380 ± 5 rpm) at some pre-selected temperatures for 2.0 hours (which was enough to achieve equilibrium). The solid adsorbent particles were filtered from the reaction mixture using 0.45-μm membrane filters. The filtrates were analyzed for fluoride remaining and final solution pH ($pH_f$). The adsorption capacity ($q_t$ or $q_e$, $mg \cdot g^{-1}$) at any time, t or at equilibrium was calculated using the equation (1) below:

$$q_t(\text{or } q_e) = [V\{C_0 - C_t(\text{or } C_e)\}]/m \quad (1)$$

where V is the volume (L) of solute solution, m the mass (g) of HICMO, and $C_0$ and $C_t$ (or $C_e$) are the concentrations ($mg \cdot L^{-1}$) of the solute at a time for agitation, t = 0 and t = t (or equilibrium), respectively.

The effect of $pH_i$ on the adsorption of fluoride by HICMO was investigated by taking $C_0$ of the solute solutions 25.0, 35.0 and 50.0 mg $F^- \cdot L^{-1}$ at pHi ranged in 3.0 to 10.0 and at temperature 298 (±1.6) K. The remaining fluoride as well as $pH_f$ of the filtered solutions was analyzed. The $q_e$ value at each designated $pH_i$ was calculated by Eq. (1).

Adsorption kinetics indicates the equilibrium time and reaction rate. Batch adsorption kinetic experiments were conducted according to the procedure described above at $pH_i = 6.5$ (±0.2) and at the temperatures (T ± 1.6) = 283, 290, 298, and 313 K taking a fixed $C_0$ of fluoride = 35.0 mg $\cdot L^{-1}$; and also by taking three different $C_0$ of fluoride (25.0, 35.0 and 50.0 mg $\cdot L^{-1}$) in solution at a fixed T = 298 (±1.6) K. The vessels with reaction mixture were taken out at some fixed interval of time, and filtered immediately after withdrawal using 0.45-μm membrane filters. The filtrates were analyzed by colorimetric method for remaining fluoride using SPADNS – $ZrOCl_2$ reagent (40).

Adsorption isotherms were investigated to describe the distribution of adsorbate between adsorbent and liquid when equilibrium state was achieved. The isotherm experiments were conducted under ambient conditions as described (agitation time: 1.5 hours) for the equilibrium at $pH_i = 6.5$ (±0.2) taking $C_0$ of fluoride ranged between 10.0 and 50.0 mg $\cdot L^{-1}$ at T (±1.6) = 288, 303, 318, and 333 K. Any change of pH was recorded after 1.0 hour of reaction and adjusted to the initial value by adding 0.1 M $HNO_3$/NaOH solution. The fluoride remained in filtered solution was analyzed (40). The adsorption capacity ($q_e$) was calculated using Eq. (1).

To investigate the competing effect of foreign ions on fluoride adsorption by HICMO, the experiments were done by batch method at conditions as mentioned above taking

50 ml solution of fluoride ($C_0 = 35.0\,mg \cdot L^{-1}$) + competing ion. The concentration range of competing ions was taken from zero $mg \cdot L^{-1}$ to a level that permitted highest by WHO in ground water.

For desorption of fluoride, 50 ml of NaOH solution were agitated ($380 \pm 5$ rpm) separately with 0.1 g fluoride adsorbed material (fluoride content $= 15.54\,mg \cdot g^{-1}$) for 1.5 hours at $T = 303$ ($\pm 1.6$) K. After 1.5 hours of agitation, the materials were separated by filtration. The filtrates were analyzed for fluoride, and the desorption percentages were calculated. To optimize the condition, the concentration of NaOH solution was varied from 0.01 to 2.0 M. To optimize agitation time, it was varied from 0.5 to 2.0 hours taking optimized NaOH concentration.

Fixed bed column experiments were conducted by uniform packing of HICMO (particle size: 140–290 μm) into two separate glass columns (i.d. 1.0 cm, length 45 cm) up to the bed heights 4.0 and 5.0 cm. The input fluoride solution ($C_0 = 7.37\,mg \cdot L^{-1}$) was passed down separately through the columns with flow rate 1.0 or $2.0\,ml \cdot min^{-1}$. The effluent was collected in 50 ml fractions, and analyzed for fluoride.

## RESULTS AND DISCUSSION

### Characterization of HICMO

The analysis of the XRD pattern of HICMO indicated that the material was amorphous. From the FTIR spectra, it was found that the absorption bands pointing maximum at the wave number between 3350 and 3450 $cm^{-1}$ were due to the O-H stretching mode of the lattice water and hydroxide group. The absorption bands found at the wave number between 1635 and 1648 $cm^{-1}$ were for the O-H bending mode of water molecules. The broad bands at around 1021–1022 $cm^{-1}$ for each of HICMO, hydrous chromium(III) oxide (HCO) and hydrous iron(III) oxide (HFO) were presumed to be the bending mode of the bridged OH group. The bands obtained at wave number (521 $cm^{-1}$) in HICMO which was lower than that of HFO (670 $cm^{-1}$) and HCO (668 $cm^{-1}$) indicated the presence of oxo/hydroxo bridge between iron(III) and chromium(III). Thus, HICMO is a hydrous bimetal mixed oxide.

The TG spectrum of HICMO was analyzed, and found the weight loss percentages were 13.37, 21.55, and 3.20 at the temperature of drying up to 70°, >70° – 270°, and >270° – 800°C, respectively. The percentages of weight loss noted correspond to the moisture content, co-ordinated water, and dehydroxylation of chelated water via hydrogen bonding and hydroxide, respectively. The steep exothermic peak at 550°C in the DT spectrum supported the observation. The $pH_{zpc}$ analyzed was 6.5 ($\pm 0.1$) for the composite oxide, which was close to neutral pH. The material was analyzed by taking the SEM image, which showed irregular surface morphology. The TEM image of the synthetic material was analyzed. It suggested that the material was agglomerated spherical nano particles (40–55 nm).

### Effect of pH

Figure 1 demonstrates the variation of (a) fluoride adsorption capacity ($q_e$, $mg \cdot g^{-1}$) of HICMO versus initial solution pH ($pH_i$), and (b) the equilibrium solution pH ($pH_f$) versus $pH_i$ for the initial fluoride concentration ($C_i$) of 25.0, 35.0 and $50.0\,mg \cdot L^{-1}$. It was found that the $q_e$ declined rapidly with rising $pH_i$ from 3.0 to 5.0, and above 7.0. The declination of $q_e$ was insignificant at $pH_i$ ranged in 5.0–7.0. The highest $q_e$ at $pH_i$ 3.0 is presumably due to the strong affinity of fluoride ion for the positive surface charge (R1) or replacement of surface hydroxide ion with fluoride (R2) of HICMO ($pH_{zpc} = 6.5 \pm 0.1$). The decrease of $q_e$

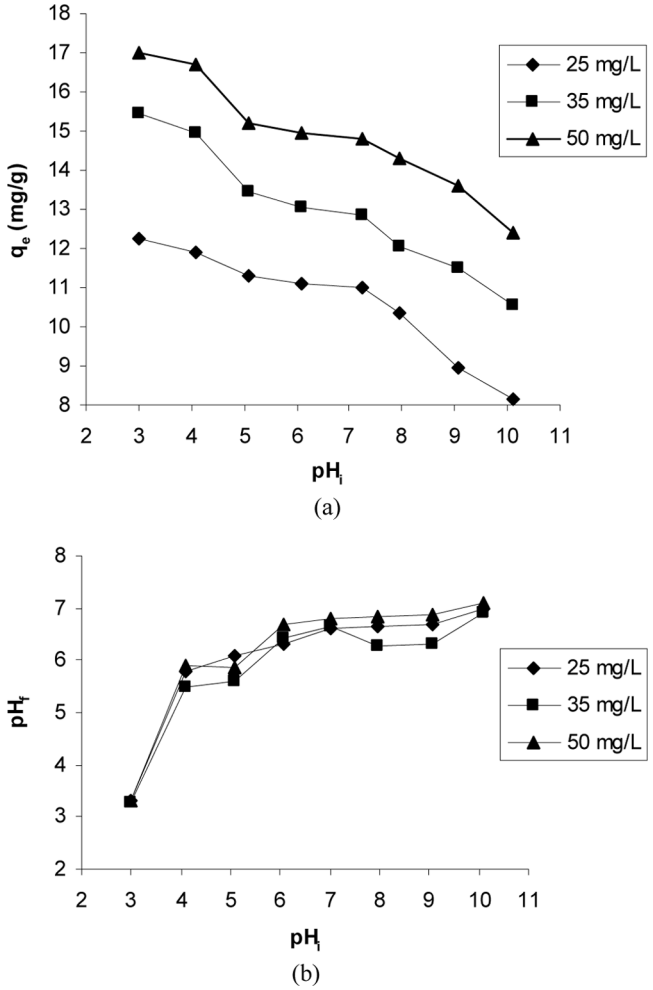


FIG. 1. The plot of (a) equilibrium adsorption capacity ($q_e$, $mg \cdot g^{-1}$) versus initial pH ($pH_i$), and (b) equilibrium solution pH ($pH_f$) versus initial pH ($pH_i$) for fluoride adsorption by HICMO at variable initial fluoride concentration at 298 ($\pm 1.6$)K.

with increasing $pH_i$ from 3.0 to 5.0 is due to the decrease of positive surface charge density or ligand exchange capacity of HICMO. The capacity at $pH_i$ between 5.0 and 7.0 was nearly same, which is presumably due to the neutral or near neutral surface of the solid as the analyzed $pH_f$ values were $6.4 \pm 0.2$ (b in Fig. 1).

$$MOH_{(S)} + H_3O^+ + F^- \rightarrow MOH_2^+ - - - F^-_{(S)} + H_2O \quad (R1)$$

$$MOH_{(S)} + H_3O^+ + F^- \rightarrow M^+ - - - F^-_{(S)} + 2H_2O \quad (R2)$$

MOH(s) stands for the solid material.

The columbic or ligand exchange type of fluoride adsorption mechanism (R1 or R2) as suggested is agreed well with the observed $pH_f$ value (b in Fig. 1). The adsorption reaction that took place at $pH_i$ between 5.0 and 7.0 is presumed to be due to the following type of surface reaction (R3). This agrees well with almost unchanged of $pH_f$ (b in Fig. 1) from $pH_i$ of the solution.

$$M - OH_{(S)} + F^-_{(aq)} \rightarrow M - O^{\partial -} - H^{\partial +}_{(s)} - - - - F^-_{(S)} \quad (R3)$$

The surface of the solid should be negative at $pH_i > pH_{zpc}$ and, the $q_e$ thus declined due to the columbic repulsion of like charges between the solute in solution and the surface of solid. The rapid decline of $q_e$ at $pH_i > 7.0$ is due to the competition of fluoride with hydroxyl ions for the secondary adsorption sphere (R4) where the $Na^+$ (available in solution) will be at the primary adsorption sphere on the solid surface.

$$M - OH_{(S)} + Na^+_{(aq)} + F^-_{(aq)} + {}^-OH_{(aq)} \rightarrow M - O^- - - Na^+ - - F^- + H_2O + aq \quad (R4)$$

$$M - OH_{(S)} + F^-_{(aq)} + OH^-_{(aq)} \rightarrow M - O^{\partial -}H^{\partial +} - - F^- + M - O^{\partial -}H^{\partial +} - - {}^-OH + aq \quad (R5)$$

From the quantitative analysis of fluoride adsorbed material, 0.13 ($\pm$0.01) mM $Na^+$ was found. However, the amount of sodium estimated was found to be less than that of adsorbed fluoride, which confirmed the mechanism (R4) partly. In addition, the adsorption mechanism could be described by the reaction noted (R5). Whatever be the case, both R4 and R5 complied the decrease of $pH_f$ from $pH_i$, and indicated the possibility of entropy increase for releasing aqua molecules at solid-liquid interface.

## Kinetic Modeling

*Effect of Concentration*

The effect of the reaction time on the adsorption rate for a $C_i$ (25.0, 35.0, and 50.0 $mg \cdot L^{-1}$) of fluoride at a temperature 298 ($\pm$1.6) K and $pH_i$ 6.5 ($\pm$0.2) is demonstrated in Fig. 2. It can be found that the $q_t$ had a rapid increase in the first 30 minutes and more than 85% of the adsorption occurred. This phenomenon may be due to rapid boundary layer diffusion of the dissolved fluoride onto the surface of the solid. The adsorption rate retards after a reaction time of 30 minutes, indicating the attainment of plateau. It is due to the columbic inhibition of fluoride adsorption by the fast growing negative surface of HICMO. The results shown in Fig. 2 had indicated that the contact time enhanced with increasing $C_i$ from 25.0 to 50.0 $mg \cdot L^{-1}$ in reaching a pseudo-equilibrium. It was about 60, 75, and 120 minutes, respectively, for the $C_i$ of 25.0, 35.0, and 50.0 $mg \cdot L^{-1}$.

The $q_t$ values shown in Fig. 2 were analyzed using the linearised equations of Lagergren pseudo-first order (1) (42), pseudo-second order (2) (43), and intra particle diffusion (3) (44) kinetics.

$$\log(q_e - q_t) = \log q_e - k_1 t/2.303 \quad (1)$$

$$t/q_t = 1/(k_2\, q_e^2) + t/q_e \quad (2)$$

$$q_t = k_{id}\, t^{0.5} + C \quad (3)$$

The significance of each term present in Eqs. (1–3) has been given in notation list.

The $q_t$ values of Fig. 2 were analyzed by the plot of

(i) log ($q_e$–$q_t$) versus t (Eq. (1)) (plot not shown),
(ii) $t/q_t$ versus t (Eq. (2)) (Fig. 3) and
(iii) $q_t$ versus $t^{0.5}$ (Eq. (3)) (plot not shown).

The parameters associated with each equation were calculated from the slopes and intercepts of the plots, which are presented in Table 1. From the correlation coefficients,

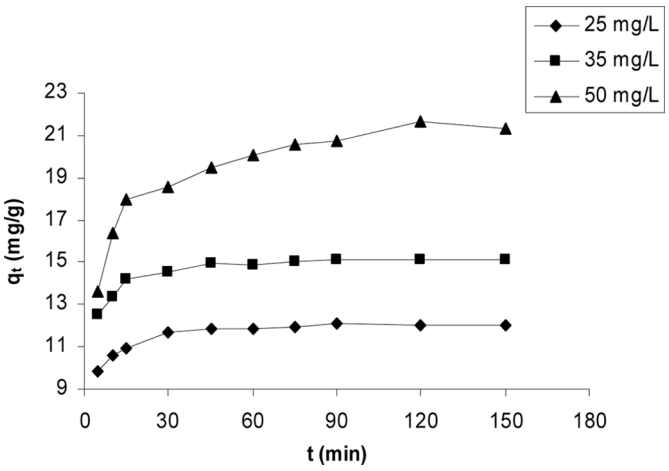


FIG. 2. The plot of fluoride adsorption capacity ($q_t$, $mg \cdot g^{-1}$) values versus time (t, min) obtained at three different solution concentrations of fluoride at pHi 6.5 ($\pm$0.2) at temperature 298 ($\pm$1.6)K.

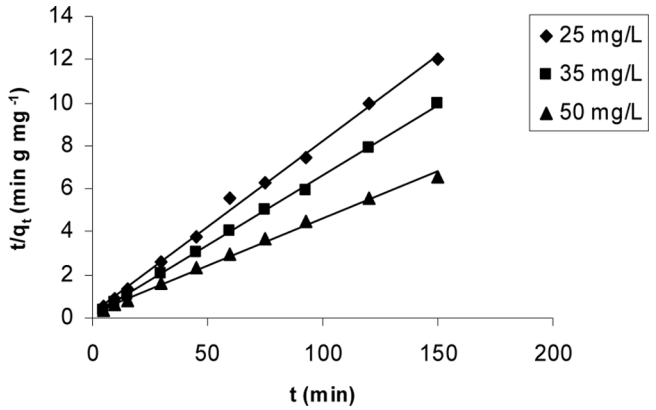


FIG. 3. The plot of $t/q_t$ ($min \cdot g \cdot mg^{-1}$) versus t (min) for the pseudo-second order kinetic analysis of the data obtained at $pH_i$ 6.5 (±0.2) and temperature 298 (±1.6)K.

it was observed that the fits of experimental data were well with the pseudo-second order equation ($r^2 = 1.00$), and better than the pseudo-first order equation ($r^2 = 0.85$–$0.95$). The pseudo-second order rate constant ($k_2$), initial adsorption affinity, $h_0$ ($= k_2 q_e^2$, $mg \cdot g^{-1} \cdot min^{-1}$), and equilibrium adsorption capacity ($q_e$) shown in Table 1 indicated that the values of $k_2$ decreased, while that of $h_0$ and $q_e$ increased with enhancing $C_i$ from 25.0 to 50.0 $mg \cdot L^{-1}$. It was found that the values of modeled $q_e$ obtained from the pseudo-second order equation were closer to the experimental $q_e$ than that from the pseudo-first order equation.

TABLE 1
The kinetics parameters estimated on fluoride adsorption by HICMO at different concentrations (temperature $298 \pm 1.6$ K and $pH_i$ $6.5 \pm 0.2$)

| Kinetic equations | Parameters | Initial fluoride concentration ($mg \cdot L^{-1}$) 25.0 | 35.0 | 50.0 |
|---|---|---|---|---|
| Pseudo-second order | $k_2 \times 10^{-2}$ ($g\ mg^{-1}\ min^{-1}$) | 7.20 | 5.25 | 3.59 |
| | $q_e$ ($mg \cdot g^{-1}$) | 11.84 | 15.27 | 20.16 |
| | $r^2$ | 1.00 | 1.00 | 1.00 |
| | $h_0$ ($mg \cdot g^{-1} \cdot min^{-1}$) | 10.09 | 12.24 | 14.59 |
| Pseudo-first order | $k_1 \times 10^{-2}$ ($min^{-1}$) | 3.66 | 4.26 | 4.12 |
| | $q_e$ ($mg \cdot g^{-1}$ | 1.56 | 2.55 | 10.32 |
| | $r^2$ | 0.94 | 0.95 | 0.85 |
| Intra particle diffusion | $k_{id} \times 10^{-1}$ ($g \cdot mg^{-1} min^{0.5}$) | 1.76 | 2.26 | 6.25 |
| | $r^2$ | 0.66 | 0.73 | 0.79 |

These aspects proved that the pseudo-second order model had described the kinetics of fluoride adsorption. The results have been found similar not only with our previous reports (35,36) but also with others (9,21). The reduction of $k_2$ value with enhancing $C_i$ is due to rapid growing of negative charge for a fast uptake of the solute on the solid surface through the boundary layer diffusion at initial stages, which retards the adsorption reaction at later stages by the electrostatic force of repulsion.

The very poor linearity ($r^2 = 0.66 - 0.79$) of the Weber-Morris plots, $q_t$ versus $t^{0.5}$ for Eq. (3) (plot not shown), had suggested that the rate determining step (RDS) of the present adsorption reaction was not solely dependent on the intra-particle (pore) diffusion of fluoride. The values of $k_{id}$ (average diffusion rate constant, $mg \cdot g^{-1}$ $min^{-0.5}$) were increased with increasing concentration (Table 1), indicating the intraparticle diffusion of solute in to the interior of adsorbent at room temperature increases. For confirming RDS, the diffusion coefficients related to the pore ($D_P$, $cm^2 \cdot s^{-1}$) (eq. 4) and the film ($D_F$, $cm^2 \cdot s^{-1}$) (eq. 5) were calculated using relations (45,46) below.

$$D_P = (0.03\ r_0^2)/t_{1/2} \quad (4)$$

$$D_F = (0.23 \times r_0 \times \partial \times C_s)/t_{1/2} \times C_L \quad (5)$$

The significance of the terms present in Eqs. (4), (5). is given in the notation list. The film thickness ($\partial$) used was 0.001 cm (45). The time (in second) for 50% reaction ($t_{1/2}$) was calculated from the relation, $t_{1/2} = 1/(q_e\ k_2)$, where $k_2$ and $q_e$ have their usual meaning and mentioned elsewhere. If the value of $D_p$ lies in $10^{-11}$ to $10^{-13}$ $cm^2 \cdot s^{-1}$, then the RDS will be controlled by pore-diffusion; and if the value of $D_F$ lies in$10^{-6}$ to $10^{-8}$ $cm^2 \cdot s^{-1}$, then the RDS will be controlled by the boundary-layer (film) diffusion (45,46). The magnitude of $D_p$ and $D_F$ values ($cm^2 \cdot s^{-1}$) calculated for the present case, respectively, were $(1.79\text{–}5.39) \times 10^{-8}$ and $(5.33 - 5.39) \times 10^{-9}$, which are not in an appropriate range described earlier. Thus, the RDS for the present case was the multistage phenomena.

*Effect of Temperature*

Figure 4 demonstrates the effect of contact time at four different reaction temperatures, T (±1.6) = 283, 290, 298, and 313 K) on the rate of fluoride adsorption by HICMO at $C_i = 35.0\ mg \cdot L^{-1}$ and $pH_i = 6.5$ (±0.2). It was found that the $q_t$ had a rapid increase in the first 20 minutes, where 85–90% of the adsorbed fluoride removal took place. After t = 20 minutes, the adsorption rate reduced. This is presumed that the initial rapid growing of negative charge on the solid surface inhibited the later stages of fluoride

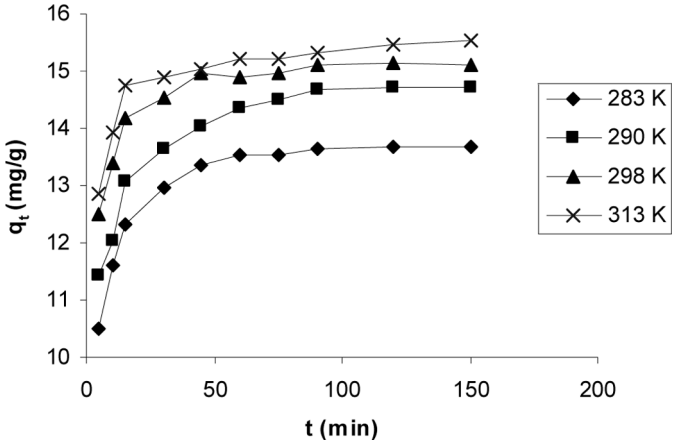


FIG. 4. The plot of adsorption capacity ($q_t$, $mg \cdot g^{-1}$) versus time (t, min) at different reaction temperatures (±1.6)K and $pH_i$ 6.5 (±0.2) for the kinetic analysis.

adsorption reaction. The $q_t$ values of Fig. 4 were analyzed by the plot of

(i) log ($q_e$– $q_t$) versus t for equation-1 (plot not shown),
(ii) $t/q_t$ versus t for Eq. (2) (Fig. 5) and
(iii) $q_t$ versus $t^{0.5}$ for Eq. (3) (plot not shown).

The parameters associated with the Eqs. (1–3) were calculated from the slopes and intercepts of respective plots, and the values are presented in Table 2. From the correlation coefficients, it was observed that the fits of experimental data were good with the pseudo-second order equation ($r^2 = 1.00$), and better than the pseudo-first order equation ($r^2 = 0.93$–$0.98$). The $q_e$ and $h_0$ values increased from 13.89 to 15.50 $mg \cdot g^{-1}$ and 7.21 to 13.11 $mg \cdot g^{-1} \cdot min^{-1}$, respectively; with increasing temperature from 283 (±1.6) to 313 (±1.6) K. Increase of $q_e$ and

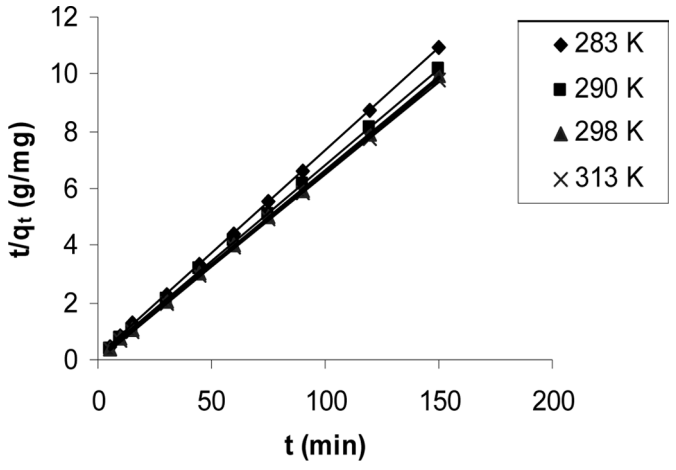


FIG. 5. The plot of $t/q_t$ ($min \cdot g \cdot mg^{-1}$) versus t (min) for the pseudo-second order kinetic analysis of the data obtained at different reaction temperature and $pH_I$ 6.5 (±0.2).

$h_0$ values (Table 2) indicated that the endothermic nature of the adsorption reaction increased with increasing temperature. In addition, the enhancement of $k_2$ ($x10^{-2}$, $g \cdot mg^{-1} \cdot min^{-1}$) (Table 2) with rising temperature from 283 (±1.6) to 313 (±1.6) K had indicated the increase of reaction rate with HICMO, which was found similar to the results that had been reported by Viswanathan and Meenakshi (37,38). The $q_t$ values against t as shown in Fig. 4 were analyzed according to the Weber-Morris plot (not shown) of Eq. (3). The regression coefficients ($r^2 = 0.73$ to 0.75) found for the $q_t$ versus $t^{0.5}$ plots were nonlinear, and the intercept, $C \neq 0$ indicated that the RDS was not controlled by the intraparticle diffusion phenomenon. The $k_{id}$-values, in general, were diminished with increasing temperature on the reaction (Table 2), indicating the decrease in dependence of kinetic rate on the intra particle diffusion.

*Activation Parameters*

Taking log on both sides with the Arrhenius activation energy Eq. (6), the activation parameters for the present reaction were computed from the slope and intercept values of the plot, $\ln k_2$ ($k_2$ = pseudo second-order rate constant) versus $T^{-1}$ ($K^{-1}$) (plot omitted) ($r^2 = 0.94$).

$$k_2 = A \exp(-E_a/RT) \tag{6}$$

The temperature independent parameter (A, $g \cdot mg^{-1} \cdot min^{-1}$) and activation energy ($E_a$, $kJ \cdot mol^{-1}$) were computed, taking R (the molar gas constant) equals to 8.314 $J \cdot mol^{-1} \cdot K^{-1}$ were 4.42 $g \cdot mg^{-1}\, s^{-1}$ and 11.12 kJ $mol^{-1}$, respectively. The values were found similar to that which had been reported by Daifullah et al. (23). The activation energy was also calculated for this reaction by inserting the $k_2$ for the temperature of 283 K and 313 K into the Eq. (7) (47).

$$\ln(k_2'/k_2) = E_a(T_2 - T_1)/RT_1T_2 \tag{7}$$

The $k_2$ and $k_2'$ are the rate constants at temperature (in K) $T_1$ and $T_2$, respectively. The value of $E_a$ calculated was 11.39 $kJ \cdot mol^{-1}$. The value of $E_a$ estimated from the slope of the said plot and that calculated using Eq. (7) (Table 3) was found below the range of 12.55–20.92 $kJ \cdot mol^{-1}$ (3–5 $kcal \cdot mol^{-1}$), a range for the internal diffusion controlled process (47). Thus, the RDS of present adsorption reaction has not been controlled by the intra particle diffusion phenomenon.

The changes of standard enthalpy of activation ($\Delta H^{\#}$), the entropy of activation ($\Delta S^{\#}$), and free energy of activation ($\Delta G^{\#}$) were estimated using the Eyring equation (8) (48).

$$\ln(k_2/T) = [\ln(k_b/h) + (\Delta S^{\#})/R] - (\Delta H^{\#})/RT \tag{8}$$

The $k_b$ and h of equation (8) are the Boltzmann and Planck constants, respectively. The activation parameters

TABLE 2
The kinetics parameters estimated on fluoride adsorption by HICMO at different temperatures (concentration 35.0 $mg \cdot F^- \cdot L^{-1}$ and $pH_i$ 6.5 ± 0.2)

| Kinetic equations | Parameters | Temperature (±1.6 K) 283 | 290 | 298 | 313 |
|---|---|---|---|---|---|
| Pseudo-second order | $k_2 \times 10^{-2}$ $(g \cdot mg^{-1} \cdot min^{-1})$ | 3.74 | 4.52 | 5.25 | 5.95 |
| | $q_e$ $(mg \cdot g^{-1})$ | 13.89 | 14.90 | 15.27 | 15.50 |
| | $r^2$ | 1.00 | 1.00 | 1.00 | 1.00 |
| | $h_0$ $(mg \cdot g^{-1} \cdot min^{-1})$ | 7.21 | 10.04 | 12.24 | 13.11 |
| Pseudo-first order | $k_1 \times 10^{-2}$ $(min^{-1})$ | 4.72 | 4.12 | 4.26 | 2.75 |
| | $q_e$ $(mg \cdot g^{-1})$ | 3.20 | 3.90 | 2.55 | 1.86 |
| | $r^2$ | 0.98 | 0.98 | 0.95 | 0.93 |
| Intra particle diffusion | $k_{id} \times 10^{-1}$ $(g \cdot mg^{-1} min^{0.5})$ | 2.78 | 3.19 | 2.26 | 2.09 |
| | $r^2$ | 0.75 | 0.83 | 0.73 | 0.71 |

related to enthalpy and entropy change ($\Delta H^{\#}$ and $\Delta S^{\#}$) were calculated from the slope and intercept of the straight line plot of $\ln(k_2/T)$ versus $1/T$ ($K^{-1}$) (plot omitted) and shown in Table 3. The change of the free energy of activation ($\Delta G^{\#}$) was calculated by using Eq. (9).

$$\Delta G^{\#} = \Delta H^{\#} - T\Delta S^{\#} \quad (9)$$

The values of $\Delta G^{\#}$ estimated were −42.39, −43.65, −45.09, and $-47.79\ kJ \cdot mol^{-1}$, respectively, at temperature 283 (±1.6), 290 (±1.6), 298 (±1.6), and 313 (±1.6) K. The increase of $-\Delta G^{\#}$ value with increasing temperature had indicated the enhancement of the spontaneous nature of fluoride adsorption by HICMO. The calculated $\Delta H^{\#}$ value was found to be + 8.64 $kJmol^{-1}$ (Table 3), which had confirmed the endothermic nature of the reaction. The positive value of $\Delta S^{\#}$ ($+180.32\ J \cdot mol^{-1} \cdot K^{-1}$) indicated that the randomness increased at solid-liquid interface during adsorption reaction onto the surface of HICMO.

## Isotherm Modeling

Figure 6 demonstrates the plot of $q_e$ $(mg \cdot g^{-1})$ against $C_e$ $(mg \cdot L^{-1})$ on fluoride adsorption by HICMO at T (±1.6) = 283, 290, 298, and 313 K and $pH_i$ = 6.5 (±0.2). The curves of different temperatures have similar trends and the equilibrium adsorption capacity ($q_e$) increased with increasing temperature. This showed that the temperature's increasing is propitious to the adsorption of fluoride on HICMO. That means that the diffusing rate and activity of fluoride ion are increscent at higher temperature, which is beneficial for fluoride ions to enter into the surface structure of HICMO. In order to understand the adsorption mechanism, the equilibrium data (Fig. 6) were analysed by the isotherm model equations viz. Langmuir (Eq. 10) (49) and Freundlich (Eq. 11) (50). The assumption based on which the Langmuir model Eq. (10) derived is monolayer adsorption of solute onto the surface of adsorbent [49], while that of the Frieundlich model Eq. (11) is an empirical description involving different sites with several adsorption energies (50).

$$q_e = \theta bC_e/(1 + bC_e) \quad (10)$$

$$q_e = K_F\ C_e^{1/n} \quad (11)$$

TABLE 3
Activation parameters estimated on fluoride adsorption by HICMO at $pH_i$ 6.5 ± 0.2

| Fluoride concentration $(mg \cdot L^{-1})$ | $r^2$ | $E_a$ $(kJ \cdot mol^{-1})$ (Eq. (8)) | $E_a$ $(kJ \cdot mol^{-1})$ (Eq. (9)) | A $(g \cdot mg \cdot min^{-1})$ | $\Delta H^{\#}$ $(kJ \cdot mol^{-1})$ | $\Delta S^{\#}$ $(J \cdot mol^{-1} \cdot K^{-1})$ | $r^2$ | Temperature (±1.6 K) | $-\Delta G^{\#}$ $(k \cdot J \cdot mol^{-1})$ |
|---|---|---|---|---|---|---|---|---|---|
| 35.0 | 0.94 | 11.12 | 11.39 | 4.42 | 8.64 | 180.32 | 0.90 | 283 | 42.39 |
| | | | | | | | | 290 | 43.65 |
| | | | | | | | | 298 | 45.09 |
| | | | | | | | | 313 | 47.79 |

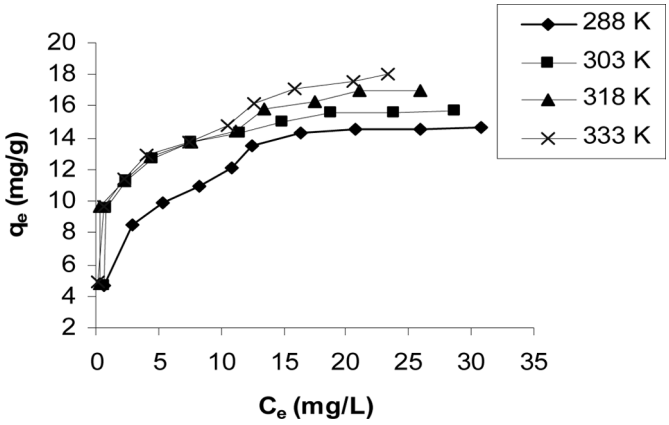


FIG. 6. The plot of fluoride adsorption capacity ($q_e$, $mg \cdot g^{-1}$) of HICMO versus equilibrium concentration ($C_e$, $mg \cdot g^{-1}$) at $pH_i$ 6.5 (±0.2) and at different temperatures (±1.6 K).

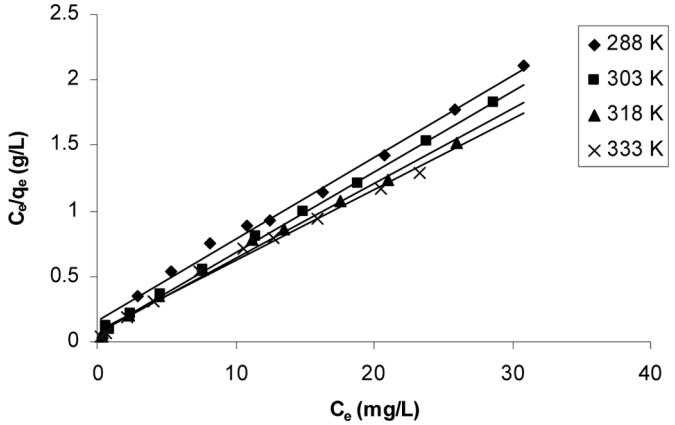


FIG. 7. The plot of $C_e/q_e(g.L^{-1})$ versus $C_e$ ($mg \cdot g^{-1}$) for linear Langmuir isotherm parameters of fluoride adsorption data obtained at different temperatures and $pH_i$ 6.5 (±0.2).

The significance of each parameter of Eqs. (10), (11). has been described in the notation list. The linearizations were made by

(i) multiplication of reversed Eq. (10) with $C_e$, and
(ii) taking log on Eq. (11), which were used for the linear analysis.

The parameters of said model Eqs. (10), (11). were computed from the linear and the nonlinear fits (best fit shown in Fig. 7) using the Microsoft computer spread sheet, and the values are shown in Table 4. From the correlation coefficients, it could be seen that the fits of equilibrium data were too well with the linear form of Langmuir equation ($r^2_{(linear)} = 0.99–1.00$) (Fig. 7) and that were superior to the nonlinear form of Langmuir equation ($r^2_{(non\text{-}linear)} = 0.89–0.96$). Again, the goodness of data fitting with either form of the Freundlich equations ($r^2_{(linear)} = 0.79–0.94$, $r^2_{(non\text{-}linear)} = 0.87–0.95$) were inferior to that of the Langmuir equations. The comparison of the computed isotherm parameters (Table 4) for different temperatures on the reaction showed that the data obtained at T = 303 (±1.6) K described the Langmuir model better ($r^2_{(linear)} = 1.00$,



TABLE 4
The estimated isotherm parameters on fluoride adsorption by HICMO at different temperatures and $pH_i$ 6.5 ± 0.2

| Isotherm models | Temperature (±1.6 K) | Linear isotherm parameters | | | Non-linear isotherm parameters | | | |
|---|---|---|---|---|---|---|---|---|
| | | $\theta(mg \cdot g^{-1})$ | $b(L \cdot mg^{-1})$ | $r^2$ | $\theta(mg \cdot g^{-1})$ | $b(L \cdot mg^{-1})$ | $r^2$ | $\chi^2$ |
| Langmuir | 288 | 15.97 | 0.39 | 0.99 | 15.88 | 0.38 | 0.95 | 0.63 |
| | 303 | 16.34 | 0.83 | 1.00 | 15.37 | 1.71 | 0.96 | 0.55 |
| | 318 | 16.42 | 1.27 | 0.99 | 15.74 | 2.15 | 0.89 | 1.58 |
| | 333 | 17.85 | 0.99 | 0.99 | 16.80 | 1.78 | 0.96 | 0.78 |
| | | $K_F$ | n | $r^2$ | $K_F$ | n | $r^2$ | $\chi^2$ |
| Freundlich | 288 | 6.64 | 4.01 | 0.94 | 6.31 | 3.73 | 0.95 | 0.63 |
| | 303 | 8.41 | 4.63 | 0.91 | 9.12 | 5.59 | 0.93 | 0.88 |
| | 318 | 8.92 | 4.78 | 0.80 | 9.62 | 5.70 | 0.87 | 1.88 |
| | 333 | 9.01 | 4.26 | 0.91 | 9.76 | 5.10 | 0.94 | 1.01 |
| | | $q_m$ ($mol \cdot kg^{-1}$) | | $\beta$ ($mol^2 \cdot kJ^{-2}$) | E ($kJ \cdot mol^{-1}$) | | $r^2$ | |
| D-R Isotherm | 303 | $1.60 \times 10^{-3}$ | | $2.0 \times 10^{-3}$ | 15.81 | | 0.95 | |

$r^2_{(non\text{-}linear)} = 0.96$) than the Freundlich model ($r^2_{(linear)} = 0.91$, $r^2_{(non\text{-}linear)} = 0.93$). Thus, the fluoride adsorption from aqueous solution by HICMO at 303 (±1.6) K and $pH_i = 6.5$ (±0.2) took place with monolayer surface coverage. The value of the Langmuir monolayer capacity ($\theta$) was between 15.37 and 16.34 $mg \cdot g^{-1}$ at T = 303 (±1.6) K, which is higher than pure iron (III) oxide (7.50 $mg \cdot g^{-1}$) (34) and that increased with increasing temperature. The Freundlich constant ($K_F$, $mg^{1-1/n}L^{1/n}g^{-1}$) values laid between 6.61 and 9.76, indicating the high affinity of HICMO for the fluoride. The Freundlich coefficient (n, dimensionless) values were between 3.73 and 5.70 that ranged in 1 to 10. This supports the favorable affinity of HICMO for fluoride. To access the effectiveness of HICMO on fluoride scavenging performance, the $\theta$ ($mg \cdot g^{-1}$) value obtained was compared with some literature available data (Table 5). It can thus be seen that the fluoride adsorption efficiency of the present mixed oxide is good in comparison to many other materials.

## Thermodynamic Parameters

Thermodynamic parameters viz. the change of Gibbs free energy, $\Delta G^0$, enthalpy, $\Delta H^0$, and entropy, $\Delta S^0$ of an adsorption reaction are used to determine spontaneity of the process and whether it is endothermic or exothermic. Higher negative value of $\Delta G^0$ reflects a more energetically favorable adsorption. The standard Eq. (12), which relates the thermodynamic parameters, was used for estimating the values.

$$\log(q_e/C_e) = \Delta S^0/2.303R - (\Delta H^0/2.303R)1/T \qquad (12)$$

Assuming $\Delta S^0$ and $\Delta H^0$ to be constant within the temperature range, the values were computed from the slope and intercept of the plot of log ($q_e/C_e$) versus 1/T (Fig. 8), and the value of $\Delta G^0$ (kJ $mol^{-1}$) was calculated by the standard relation (47) at the reaction temperatures. The plots shown in Fig. 8 had high regression coefficients ($r^2 = 0.99$). The thermodynamic parameters computed for

TABLE 5
The comparative assessment of Langmuir monolayer adsorption capacity ($\theta$, $mg \cdot g^{-1}$) of HICMO with some other recent developed defluoridation media

| Adsorbent | $\theta$ ($mg \cdot g^{-1}$) | Experimental conditions | Reference |
|---|---|---|---|
| Algal biosorbent Spirogyra sp.-IO2 | 1.27 | pH = 7.0<br>Concentration: 5–25 $mg \cdot L^{-1}$ | 27 |
| $KMnO_4$-modified carbon | 15.90 | pH = 2<br>Concentration: 5–20 $mg \cdot L^{-1}$ | 23 |
| Plaster of Paris | 0.336 | pH = 3–9<br>Concentration: 2–10 $mg \cdot L^{-1}$ | 22 |
| Light weight concrete material | 5.15 | pH = 8.9<br>Concentration range: probably 10–50 $mg \cdot L^{-1}$ | 21 |
| Magnetic-chitosan | 22.49 | pH = 7<br>Concentration: 5–40 $mg \cdot L^{-1}$ | 19 |
| Iron-Zirconium hybrid oxide | 8.21 | pH = 6.8 ± 0.1<br>Concentration: 5–50 $mg \cdot L^{-1}$ | 34 |
| Iron-Aluminum mixed oxide | 17.73 | pH = (6.9 ± 02)<br>Concentration: 10–50 $mg \cdot L^{-1}$ | 35 |
| Iron-Tin mixed oxide | 10.47 | pH = (6.4 ± 0.2)<br>Concentration: 10–50 $mg \cdot L^{-1}$ | 36 |
| Quick lime | 16.67 | pH = 6.61<br>Concentration: 10–50 $mg \cdot L^{-1}$ | 18 |
| La(III) incorporated carboxylated chitosan beads | 11.91 | pH = 7<br>Concentration: 11–19 $mg \cdot L^{-1}$ | 37 |
| Fe(III) loaded carboxylated chitosan beads | 15.39 | pH = 7<br>Concentration: 11–19 $mg \cdot L^{-1}$ | 38 |
| Fe(III)-LECCA | 18.55 | pH = 5.6<br>Concentration: 10–200 $mg \cdot L^{-1}$ | 39 |
| Iron-Chromium mixed oxide | 16.34 | pH = 6.5<br>Concentration: 10–50 $mg \cdot L^{-1}$ | Present work |

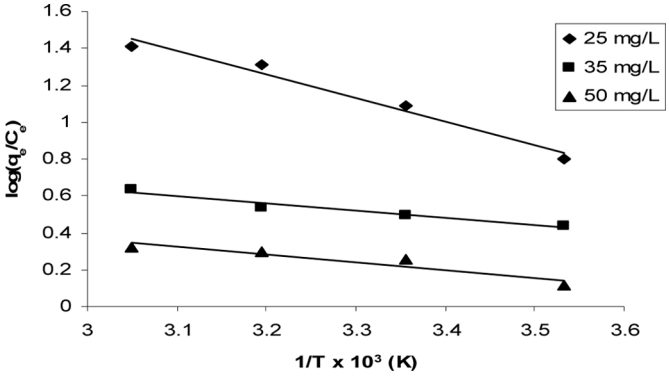


FIG. 8. The plot of log ($q_e/C_e$) versus (1/T) for thermodynamic parameters for fluoride adsorption onto HICMO surface at $pH_i$ 6.5 (±0.2).

the present reaction using fluoride solution of $C_i = 25.0$, 35.0, and 50.0 $mg \cdot L^{-1}$ are given in Table 6. The positive $\Delta H^0$ ($kJ \cdot mol^{-1}$) values indicated that the fluoride adsorption reaction with HICMO was endothermic. The lowering of $\Delta H^0$ with increasing $C_i$ indicated that the reaction tends to be less endothermic at a higher level of fluoride in solution. The values of $\Delta S^0$ were +101.86, +34.70 and +30.80 $J \cdot mol^{-1} \cdot K^{-1}$, respectively, for the $C_i = 25.0$, 35.0, and 50.0 mg $F^- \cdot L^{-1}$. This had indicated that the fluoride adsorption by HICMO took place with increasing entropy. This is presumably for the increase of randomness at solid–liquid interface due to the release of

(i) aqua molecules, and
(ii) hydroxide ion from the solid surface when the solvated fluoride distributed from the aqueous solution onto the solid. The $-\Delta G^0$ values (Table 6) for the temperatures 283, 298, 313, and 328 K had confirmed that this reaction was a spontaneous process.

It can also be seen that the $-\Delta G^0$ values are progressively higher (Table 6) with increasing temperature on the reaction from 283 to 328 K. This indicated that the spontaneity of the reaction was enhanced with increasing temperature for a definite fluoride load with HICMO. It was seen that the magnitude of $-\Delta G^0$ reduced with increasing fluoride load per g of solid, indicating the decrease of reaction spontaneity. This is presumably due to the columbic inhibition of fluoride adsorption at later stages by the fast grown negative surface on the solid at initial stages of rapid uptake.

## Adsorption Energy

The magnitude of mean free energy of adsorption ($E_{DR}$, $kJ \cdot mol^{-1}$) is useful in predicting the type of adsorption reaction. If the $E_{DR}$ value is in the range of 8.0–16.0 $kJ \cdot mol^{-1}$, the adsorption reaction should take place with ion-exchange mechanism (23,51). To evaluate it, the equilibrium data demonstrated in Fig. 6 were analyzed by the Dubinin-Radushkevick (D-R) Eq. (13) (51).

$$\ln q_e = \ln q_m - \beta\varepsilon^2 \tag{13}$$

The polanyi potential ($\varepsilon$) was calculated by the relation (14),

$$\varepsilon = RT\ \ln(1 + 1/C_e) \tag{14}$$

The significance of each term has been given elsewhere. The values of $q_m$ and $\beta$ were evaluated from the intercepts and slopes of the plots of ln $q_e$ versus $\varepsilon^2$ (Fig. 9). The mean free energy of adsorption ($E_{DR}$) is the free energy change when one mole of a solute is transferred to the surface of the adsorbent from infinity in solution (51), and that was calculated by Eq. (15).

$$E_{DR} = 1/(2\beta)^{1/2} \tag{15}$$

The D–R parameters and the $E_{DR}$ value evaluated are shown in Table 4. In the present case, the $E_{D-R}$ value analyzed was 15.81 $kJ \cdot mol^{-1}$ which is ranged in 8.0–16.0 $kJ \cdot mol^{-1}$. This had indicated that the fluoride adsorption by HICMO took place with ion-exchange mechanism.

## Effect of Competing Ions

The competing ions with fluoride for adsorption sites of the adsorbent should reduce efficiency of the material. The ions viz. calcium, magnesium, chloride, sulfate, phosphate, and bicarbonate are generally present at high level

TABLE 6
Thermodynamic parameters estimated on fluoride adsorption by HICMO at different temperatures and $pH_i$ 6.5 ± 0.2

| Fluoride concentration ($mg \cdot L^{-1}$) | $\Delta H^0$ ($kJ \cdot mol^{-1}$) | $\Delta S^0$ ($J \cdot mol^{-1} \cdot K^{-1}$) | $r^2$ | $-\Delta G^0$ ($kJ \cdot mol^{-1}$) at temperature (±1.6 K) | | | |
|---|---|---|---|---|---|---|---|
| | | | | 283 | 298 | 313 | 328 |
| 25.0 | +24.31 | +101.86 | 0.97 | 4.52 | 6.05 | 7.39 | 9.10 |
| 35.0 | +7.45 | +34.70 | 0.95 | 2.37 | 2.89 | 3.14 | 3.93 |
| 50.0 | +7.95 | +30.80 | 0.88 | 0.83 | 1.23 | 1.69 | 2.15 |

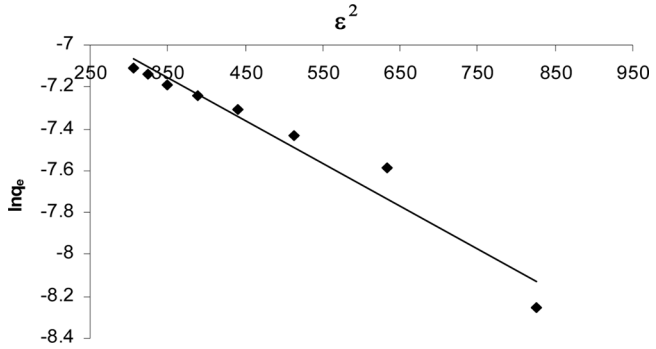


FIG. 9. The plot of Dubinin–Radushkevich (D-R) isotherm for the fluoride adsorption reaction onto HICMO surface at $pH_i$ 6.5 (±0.2) and 303 (±1.6)K.

in groundwater, and used for testing their influence on fluoride removal by HICMO. It was found that all the ions, excepting bicarbonate, showed slight negative influence on the fluoride removal of HICMO. The bicarbonate when present at high level ($400.0\,mg \cdot L^{-1}$) with fluoride in aqueous solution showed a negative influence on the fluoride removal efficiency of HICMO. It reduced the $q_e$ from $15.03\,mg \cdot g^{-1}$ (zero bicarbonate) to $13.25\,mg \cdot g^{-1}$ ($400.0\,mg\ HCO_3^- \cdot L^{-1} + 35.0\,mg\ F^- \cdot L^{-1}$). Thus, the bicarbonate, if present at high level in natural water, should reduce the fluoride removal performance of HICMO by an amount of 12–13%.

## Desorption Study

Results of pH effect on fluoride adsorption by HICMO showed (as in Fig. 1) that the $q_e$ reduced in strong alkaline pH. Based on that observation, the desorption of fluoride from the adsorbed solid ($F^-$ content: $15.54\,mg \cdot g^{-1}$ HICMO) was conducted by batch experiments with differing solution pH from 10.0 to 14.0, which showed that the solution of pH 14.0 (1.0 M NaOH) could desorb >90% of the $q_e$ from the solid surface. When the concentration of NaOH solution was varied for optimizing, it was found that the desorption percentages of fluoride had increased from 64.24 to 91.00 with increasing concentration of NaOH from 0.01 to 0.5 M, and that was nearly the same when the alkali concentration was increased up to 1.5 M. Thus, it can be suggested that the NaOH solution of concentration 0.50 M is optimum for desorbing (~91.0% fluoride) fluoride from adsorbed HICMO. The remaining ~9% fluoride could not be possible to remove from the solid surface. This ~9% of $q_e$ is presumed to be present at the interior pore surface of the solid which could be impossible to replace by the bulky aquated hydroxyl ion of alkali. The results on optimization of agitation time experiments showed that the agitation time required was 1.0 to 1.25 hours for the maximum possible desorption of fluoride.

## Fixed Bed Column Study

Figure 10 demonstrates the breakthrough curves on fluoride removal from the solution ($C_0 = 7.37\,mg \cdot F^- \cdot L^{-1}$) by HICMO column with variation of (a) flow rate and (b) bed height. The data shown in Fig. 10 were analyzed using Eqs. (16)–(19) of the adsorption zone theory (52).

$$Q_B = (C_0 \times V_B)/M \tag{16}$$

$$Q_T = Q_z/M + Q_B \tag{17}$$

$$F = Q_z/[C_0 \times (V_T - V_B)] \tag{18}$$

$$Hz = [H_T \times (V_T - V_B)]/[V_T - (1 - F)] \times (V_T - V_B) \tag{19}$$

The significance of the terms associated with Eqs. (16)–(19). has been given in the notation list. The column parameters estimated by analyzing the breakthrough data using

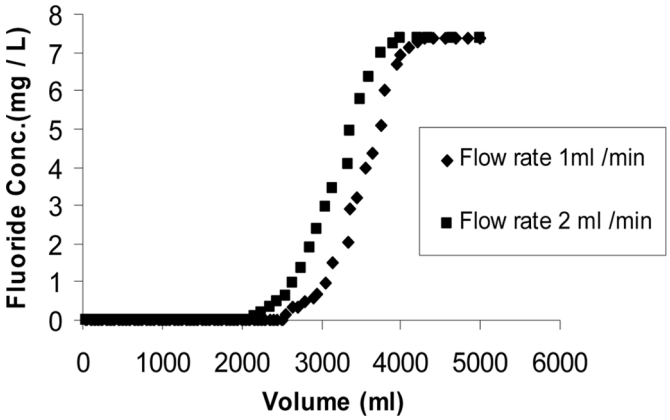


(a)

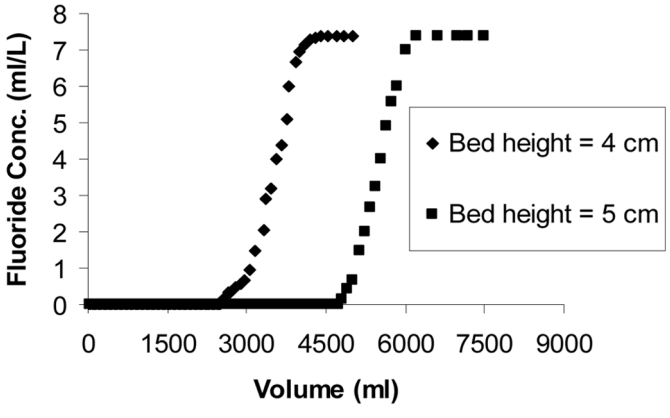


(b)

FIG. 10. The small scale fixed bed column test on fluoride removal with variation of (a) effluent flow rate and (b) bed height.

TABLE 7
Column parameters estimated on fluoride adsorption by HICMO at $pH_i$ $6.5 \pm 0.2$

| | Flow rate ($ml \cdot min^{-1}$) | | Column bed height (cm) (Flow rate $1.0\,ml \cdot min^{-1}$) | |
|---|---|---|---|---|
| Parameters | 1.0 | 2.0 | 4.0 | 5.0 |
| $V_B$ (ml) | $3.0 \times 10^3$ | $2.6 \times 10^3$ | $3.0 \times 10^3$ | $5.1 \times 10^3$ |
| $V_T$ (ml) | 4000 | 3700 | 4000 | 6000 |
| $Q_B$ ($mg \cdot g^{-1}$) | 7.37 | 6.38 | 7.37 | 9.42 |
| $Q_T$ ($mg \cdot g^{-1}$) | 9.83 | 8.51 | 9.83 | 11.78 |
| f | $1.0 \times 10^{-3}$ | $2.1 \times 10^{-3}$ | $1.0 \times 10^{-3}$ | $1.42 \times 10^{-3}$ |
| $H_T$ (cm) | 4 | 4 | 4 | 5 |
| $H_z$ | 1.32 | 1.69 | 1.32 | 0.89 |

Eqs. (16)–(19) are shown in Table 7. It had been found that the $Q_B$ and $Q_T$ reduced from 7.37 and $9.83\,mg \cdot g^{-1}$ to 6.38 and $8.51\,mg \cdot g^{-1}$, respectively, for enhancing the flow rate of the effluent from 1.0 to $2.0\,ml \cdot min^{-1}$ for a column of bed volume (BV) $3.14\,cm^3$ and $C_0$ of fluoride $7.37\,mg \cdot L^{-1}$. In addition, the value of $Q_B$ and $Q_T$ had increased from 7.37 and $9.83\,mg \cdot g^{-1}$ to 9.42 and $12.08\,mg \cdot g^{-1}$ with increasing BV of column from 3.14 to $3.93\,cm^3$, respectively. The increase of $Q_B$ and $Q_T$ proportionated approximately with the increasing bed height or BV. The other parameters obtained from the column analysis are also listed in Table 7.

## CONCLUSION

Investigation of fluoride removal efficiency of synthetic HICMO ($pH_{zpc} = 6.5 \pm 0.1$) showed that the adsorption capacity declined with increasing solution pHi from 3.0 to 5.0, and that remained nearly same up to $pH_i$ 7.0. The adsorption kinetics was the pseudo-second-order type. The equilibrium data described the Langmuir model. The monolayer adsorption capacity estimated was 16.34 ($\pm 0.50$) $mg \cdot g^{-1}$ at 303 ($\pm 1.6$) K. The ion-exchange mechanism was suggested for the fluoride adsorption reaction from the mean adsorption energy ($E_{D-R} = 15.81 kJ \cdot mol^{-1}$). The adsorption reaction was endothermic and spontaneous. The high bicarbonate reduced the fluoride removal efficiency of HICMO. The 0.5 M NaOH solution could release ~91% of the adsorbed fluoride from the material. The breakthrough capacity ($mg \cdot g^{-1}$) of HICMO packed fixed bed reduced 13–14% with enhancing flow rate of fluoride solution ($C_0 = 7.37\,mg \cdot L^{-1}$) from 1.0 to $2.0\,ml.min^{-1}$.

## ACKNOWLEDGEMENT

The authors acknowledge sincerely to the Ministry of Water Resources and Central Groundwater Board for the financial support, and are also grateful to the Principal, Presidency College and the Head, Department of Chemistry, Presidency College, Kolkata, India for laboratory facilities.

## NOTATIONS

| | |
|---|---|
| HICMO | Hydrous iron(III)-chromium(III) mixed oxide |
| T | Absolute temperature (K) |
| $E_a$ | Energy of activation ($kJ \cdot mol^{-1}$) for the reaction |
| $q_t$ | Adsorption capacity ($mg \cdot g^{-1}$) at any time (t, min) |
| $q_m$ | Adsorption capacity ($mol \cdot kg^{-1}$) of D–R equation |
| $C_t$ | Fluoride concentration in solution ($mg \cdot L^{-1}$) at any time (t, min) |
| $C_L$ | Fluoride concentration in liquid phase ($mg \cdot L^{-1}$) at time, $t = 0$ |
| $C_s$ | Fluoride concentration in solid phase ($mg \cdot g^{-1}$) at equilibrium |
| $\beta$ | A constant of D–R isotherm equation ($mol^2 \cdot kJ^{-2}$) |
| D–R | Dubinin–Radushkevick isotherm equation |
| $q_e$ | Equilibrium adsorption capacity ($mg \cdot g^{-1}$) |
| b | Langmuir isotherm equilibrium constant ($L \cdot mg^{-1}$) |
| $C_e$ | Fluoride concentration ($mg \cdot L^{-1}$) in solution at equilibrium |
| $D_F$ | Film diffusion coefficient ($cm^2 \cdot s^{-1}$) |
| $\partial$ | Film thickness (cm) |
| n | Freundlich isotherm constant (dimensionless) |
| $K_F$ | Freundlich isotherm constant ($mg^{1-1/n}L^{1/n}g^{-1}$) |
| $h_0$ | Initial adsorption rate ($mg \cdot g^{-1} \cdot time^{-1}$) |
| $C_i$ | Initial fluoride concentration ($mg \cdot L^{-1}$) in solution when time, $t = 0$ |
| C | Diffusion constant which measures the film thickness |
| $k_{id}$ | Intra-particle (pore) diffusion rate constant ($mg \cdot g^{-1}$. $time^{-0.5}$) |

| | |
|---|---|
| $\theta$ | Langmuir monolayer adsorption capacity ($mg \cdot g^{-1}$) |
| $r^2$ | Linear regression co-efficient |
| m | Mass of solid (adsorbent) added (g) |
| $E_{DR}$ | Mean free energy of adsorption ($kJ \cdot mol^{-1}$) |
| $r_0$ | Mean radius of adsorbent particles (cm) (assumed spherical) |
| $\varepsilon$ | Polanyi potential |
| $D_P$ | Pore-diffusion coefficient ($cm^2 \cdot s^{-1}$) |
| $k_1$ | Pseudo-first order rate constant ($time^{-1}$) |
| $k_2$ | Pseudo-second order rate constant ($g \cdot mg^{-1} \cdot min^{-1}$) |
| V | Solution volume (L) |
| $\Delta H^0$ | Standard enthalpy change ($kJ \cdot mol^{-1}$) |
| $\Delta S^0$ | Standard entropy change ($J \cdot mol^{-1} \cdot K^{-1}$) |
| $\Delta G^0$ | Standard Gibbs free energy change ($kJ \cdot mol^{-1}$) |
| A | Temperature- independent factor ($g \cdot mg^{-1} \cdot min^{-1}$) |
| t | Time (min) |
| $t_{1/2}$ | Time (sec) for 50% adsorption |
| R | Universal molar gas constant ($8.314\,J \cdot mol^{-1} \cdot K^{-1}$) |
| ZPC | Zero point charge |
| $K_b$ | Boltzmann constant ($1.3805 \times 10^{-23}\,J \cdot K^{-1}$) |
| h | Planck constant ($6.6256 \times 10^{-34}\,J \cdot s$) |
| $\Delta H^{\neq}$ | Standard enthalpy change ($kJ \cdot mol^{-1}$) of activation |
| $\Delta S^{\neq}$ | Standard entropy change ($J \cdot mol^{-1} \cdot K^{-1}$) of activation |
| $\Delta G^{\neq}$ | Standard Gibbs free energy change ($kJ \cdot mol^{-1}$) of activation |
| $V_B$ | Effluent volume (ml) at breakthrough point |
| $V_T$ | Effluent volume (ml) at saturation point |
| $C_0$ | Influent fluoride concentrations ($mg \cdot L^{-1}$) |
| M | Mass (g) of adsorbent packed in column |
| $Q_B$ | Mean adsorption capacity ($mg \cdot g^{-1}$) at breakpoint in column |
| $Q_T$ | Mean adsorption capacity ($mg \cdot g^{-1}$) at column saturation point |
| $Q_Z$ | Adsorption capacity ($mg \cdot g^{-1}$) of adsorption zone in column |
| F | Fraction of the adsorbent bed used to form adsorption zone |
| $H_Z$ | Height (cm) of adsorption zone formed in column |
| $H_T$ | Height (cm) of adsorbent bed in column |



## REFERENCES


1. Susheela, A.K. (1999) Flurosis management programme in India. *Current Sci.*, 77 (10): 1250.
2. Saxena, V.K.; Ahmed, S. (2001) Dissolution of fluoride in groundwater: A water-rock interaction study. *Environ. Geol.*, 40 (9): 1084.
3. Yang, C.L.; Dluhy, R. (2002) Electrochemical generation of aluminium sorbent for fluoride adsorption. *J. Hazard. Mate.*, 94 (3): 239.
4. Reardon, E.J.; Wang, Y.A. (2000) Limestone reactor for fluoride removal from waste waters. *Environ. Sci. Technol.*, 34 (15): 3247.
5. Li, Y.H.; Wang, S.; Cao, A.; Zhao, D.; Zhang, X.; Xu, C.; Luan, Z.; Ruan, D.; Liang, J.; Wu, D.; Wei, B. (2001) Adsorption of fluoride from water by amorphous alumina supported on carbon nanotubes. *Chem. Phys. Lett.*, 350 (5–6): 412.
6. Srimurali, M.; Pragathi, A.; Karthikeyan, J.A. (1998) Study on removal of fluoride from drinking water by adsorption onto low cost materials. *Environ. Pollut.*, 99 (2): 285.
7. Yang, M.; Hashimoto, T.; Hoshi, N.; Myoga, H. (1999) Fluoride removal in a fixed bed packed with granular calcite. *Water Res.*, 33 (16): 3395.
8. Piekos, R.; Paslawaska, S. (1999) Fluoride uptake characteristic of fly ash. *Fluoride*, 32 (1): 14.
9. Wasay, A.S.; Haron, Md. J.; Tokunaga, S. (1996) Adsorption of fluoride, phosphate and arsenate ions on lanthanum impregnated silica gel. *Water Environ. Res.*, 68 (3): 295.
10. Cengeloglu, Y.; Kir, E.; Ersoz, M. (2002) Removal of fluoride from aqueous solution by using red mud. *Sep. Purif. Technol.*, 28 (1): 81.
11. Fan, X.; Parker, D.J.; Smith, M.D. (2003) Adsorption kinetics of fluoride on low cost materials. *Water Res.*, 37 (20): 4929.
12. Jamode, A.V.; Sapkal, V.S.; Jamode, V.S. (2004) Defluoridation of water using inexpensive adsorbents. *J. Ind. Inst. Sci.*, 84: 163.
13. Maharamanlioglu, M.; Kizilcikli, I.; Bicer, I.O. (2002) Adsorption of fluoride from aqueous solution by acid treated spent bleaching earth. *J. Fluorine Chem.*, 115 (1): 41.
14. Zhou, Y.; Yu, C.; Shan, Y. (2004) Adsorption of fluoride from aqueous solution on $La^{3+}$-impregnated cross-linked gelatin. *Sep. Purif. Technol.*, 36 (2): 89.
15. Liao, X.P.; Shi, B. (2005) Adsorption of fluoride on zirconium(IV)-impregnated collagen fibre. *Environ. Sci. Technol.*, 39 (12): 4628.
16. Das, N.; Pattanaik, P.; Das, R. (2005) Defluoridation of drinking water using activated titanium rich bauxite. *J. Colloid. Interface Sci.*, 292 (1): 1.
17. Sarkar, M.; Banerjee, A.; Pramanik, P.P.; Sarkar, A.R. (2006) Use of laterite for the removal of fluoride from contaminated drinking water. *J. Colloid. Interface Sci.*, 302 (2): 432.
18. Islam, M.; Patel, R.K. (2007) Evaluation of removal efficiency of fluoride from aqueous solution using quick-lime. *J. Hazard. Mate.*, 143 (1–2): 303.
19. Ma, W.; Ya, F.Q.; Han, M.; Wang, R. (2007) Characteristic of equilibrium kinetics studies for the adsorption of fluoride on magnetic-chitosen particle. *J. Hazard. Mate.*, 143 (1–2): 296–302.
20. Tor, A. (2006) Removal of fluoride from aqueous solution by using montmorillonite. *Desalination*, 201 (1–3): 267.
21. Oguz, E. (2007) Equilibrium isotherms and kinetics studies for the sorption of fluoride on light weight concrete materials. *J. Colloid and surfaces A: Physicochem. Eng. Aspects*, 295: 258.
22. Gopal, V.; Elango, K.P. (2007) Equilibrium kinetics and thermodynamics studies of adsorption of fluoride onto plaster of paris. *J. Hazard. Mate.*, 141 (1): 98.
23. Daifullah, A.A.M.; Yakout, S.M., Elreefy, S.A. (2007) Adsorption of fluoride in aqueous solutions using $KMnO_4$ – modified activated carbon derived from stem pyrolysis of rich straw. *J. Hazard. Mate.*, 147 (1–2): 633.
24. Sarkar, M.; Banerjee, A.; Pramanik, P.P. (2006) Kinetics and mechanism of fluoride removal using laterite. *Ind. Eng. Chem. Res.*, 45: 5920.
25. Kamble, S.P.; Jagtap, S.; Labhsetwar, M.K.; Thakare, D.; Godfrey, S.; Tevotta, S.; Rayalu, S.S. (2007) Defluoridation of drinking water using Chitin, Chitosan and lanthanum-modified chitosan. *Chem. Eng. J.*, 129 (1–3): 173.

26. Maliyekkal, S.M.; Sharma, A.K; Philip, L. (2006) Manganese oxide-coated alumina: a promising sorbent for defluoridation of water. *Water Res.*, 40 (19): 3497.
27. Mohan, S.V.; Ramanaiah, S.V.; Rajkumar, B.; Sarma, P.N. (2007) Removal of fluoride from aqueous phase by biosorption on to algal biosorbent spirogyra Sp.– 102: sorption mechanism elucidation. *J. Hazard. Mate.*, 141 (3): 465.
28. Das, D.P.; Das, J.; Parida, K. (2003) Physicochemical characterization and adsorption behavior on calcined Zn/Al hydrotalcite – like compound (HTlc) towards removal of fluoride from aqueous solution. *J. Colloid Interface Sci.*, 261 (2): 213.
29. Wu, X.; Zhang, Y.; Dou, X.; Yang, M. (2007) Fluoride removal performance of a novel Fe-Al-Ce trimetal oxide adsorbent. *Chemosphere*, 69 (11): 1758.
30. Ghorai, S.; Pant, K.K. (2004) Investigation on the column performance of fluoride adsorption by activated alumina in a fixed bed. *Chem. Eng. J.*, 98 (1–2): 165.
31. Abe, I.; Iwasaki, S.; Tokimoto, T.; Kawasaki, N.; Nakamura, T.; Tanada, S. (2004) Adsorption of fluoride ions onto carbonaceous materials. *J. Colloid Interface Sci.*, 275 (1): 35.
32. Dey, S.; Goswami, S.; Ghosh, U.C. (2004) Hydrous ferric oxide – A scavenger of fluoride from contaminated water. *Water Air Soil Pollu.*, 158 (1): 311.
33. Goswami, S.; Dey, S.; Ghosh, U.C. (2004) Studies on removal of fluoride by hydrated zirconium oxide. *Chem. Environ. Res.*, 13 (1–2): 117.
34. Biswas, K.; Bandhoyapadhyay, D.; Ghosh, U.C. (2007) Adsorption kinetics of fluoride on iron(III)-zirconium(IV) hybrid oxide. *Adsorption*, 13 (1): 83.
35. Biswas, K.; Saha, S.K.; Ghosh, U.C. (2007) Adsorption of fluoride from aqueous solution by a synthetic iron (III) – aluminum (III) mixed oxide. *Ind. Eng. Chem. Res.*, 46 (16): 5346.
36. Biswas, K.; Gupta, K.; Ghosh, U.C. (2008) Adsorption of fluoride by hydrous iron (III)-tin(IV) bimetal mixed oxide from the aqueous solution. *Chem. Eng. J.*, 149 (1–3): 196.
37. Viswanathan, N.; Meenakshi, S. (2008) Enhanced fluoride sorption using La(III) incorporated carboxylated chitosan beads. *J. Colloid Interface Sci.*, 322 (2): 375.
38. Viswanathan, N.; Meenakshi, S. (2008) Selective sorption of fluoride using Fe (III) loaded carboxylated chitosan beads. *J. Fluorine Chem.*, 129 (6): 503.
39. Zhao, Y.; Li, X.; Liu, L.; Chen, F. (2008) Fluoride removal by Fe(III)-loaded ligand exchange cotton cellulose adsorbent from drinking water. *Carbohydrate Polymer*, 72 (1): 144.
40. APHA, AWWA, WEF. (1998) Standard Methods for the Examination of Water and Wastewater. In: *Inorganic nonmetallic constituents,* 20th Ed.; Clesceri, L.S.; Greenberg, A.E.; Eaton, A.D., eds.; Washington, DC, 4–82.
41. Babic, B.M.; Milonjic, S.K.; Polovina, M.J.; Kaludierovic, B.V. (1999) Point of zero charge and intrinsic equilibrium constants of activated carbon cloth. *Carbon*, 37 (3): 477.
42. Lagergren, S. (1898) Zur theorie der sogenannten adsorption gelöster stoffe. Kungliga Svenska Vetenskapsakademiens. *Handlingar*, 24 (1): 1.
43. Ho, Y.S.; McKay, G. (1998) Kinetic model for lead (II) sorption onto peat. *Adsorp. Sci. Technol.*, 16: 243.
44. Weber, Jr. W.J.; Morriss, J.C. (1963) Kinetics of adsorption on carbon from solution. *J. Sanit. Div. Am. Soc. Civ. Eng.*, 89 (1): 31.
45. Helfferich, F. (1962) *Ion Exchange*; McGraw-Hill: New York.
46. Michelson, L.D.; Gideon, P.G.; Pace, E.G.; Kutal, L.H. (1975) Removal of soluble mercury from wastewater by complexing techniques. Bulletin No. 74; Industry Office of Water Research and Technology, U. S. Department of Energy; Washington, DC.
47. Faust, S.D.; Aly, O.M. (1987) *Adsorption Process for Water Treatment*; Butterworths Publisher, London.
48. Anirudhan, T.S.; Radhakrishnan, P.G. (2008) Thermodynamics and kinetics of adsorption of Cu (II) from aqueous solutions onto a new cation exchanger derived from tamarind fruit shell. *J. Chem. Thermo.*, 40 (4): 702.
49. Langmuir, I. (1916) The constitution and fundamental properties of solids and liquids. part I. solids. *J. Am. Chem. Soc.*, 38 (11): 2221.
50. Freundlich, H.M.F. (1906) Über die adsorption in lössungen. *Z. Phys. Chem. (Leipzig)*, 57A: 385.
51. Dubinin, M.M.; Radushkevich, L.V. (1947) *Proc. Acad. Sci. Phys. Chem. Sect. (USSR.)*, 55: 331.
52. Jiang, Z.; Qing, C.; Song, Z. (1992) *Engineering of Ion Exchange and Separation*; Tianjing University Publication: China.